



# Artificial intelligence exploration of unstable protocells leads to predictable properties and discovery of collective behavior

Laurie J. Points<sup>a</sup>, James Ward Taylor<sup>a</sup>, Jonathan Grizou<sup>a</sup>, Kevin Donkers<sup>a</sup>, and Leroy Cronin<sup>a,1</sup>

<sup>a</sup>WestCHEM, School of Chemistry, University of Glasgow, Glasgow G12 8QQ, United Kingdom

Edited by Robert H. Austin, Princeton University, Princeton, NJ, and approved December 4, 2017 (received for review June 19, 2017)

Protocell models are used to investigate how cells might have first assembled on Earth. Some, like oil-in-water droplets, can be seemingly simple models, while able to exhibit complex and unpredictable behaviors. How such simple oil-in-water systems can come together to yield complex and life-like behaviors remains a key question. Herein, we illustrate how the combination of automated experimentation and image processing, physicochemical analysis, and machine learning allows significant advances to be made in understanding the driving forces behind oil-in-water droplet behaviors. Utilizing >7,000 experiments collected using an autonomous robotic platform, we illustrate how smart automation cannot only help with exploration, optimization, and discovery of new behaviors, but can also be core to developing fundamental understanding of such systems. Using this process, we were able to relate droplet formulation to behavior via predicted physical properties, and to identify and predict more occurrences of a rare collective droplet behavior, droplet swarming. Proton NMR spectroscopic and qualitative pH methods enabled us to better understand oil dissolution, chemical change, phase transitions, and droplet and aqueous phase flows, illustrating the utility of the combination of smart-automation and traditional analytical chemistry techniques. We further extended our study for the simultaneous exploration of both the oil and aqueous phases using a robotic platform. Overall, this work shows that the combination of chemistry, robotics, and artificial intelligence enables discovery, prediction, and mechanistic understanding in ways that no one approach could achieve alone.

artificial intelligence | protocell models | complex chemical systems | emergence | machine learning

There is great interest in oil-in-water droplets both as protocell models and as simple systems that display an astonishingly delicate set of behaviors that rest on a sensitive knife edge between stability and instability (1). They have been shown to exhibit cell-like properties including movement, division, and chemotaxis while inherently satisfying the need for a protocell to be compartmentalized (2–5). The understanding of the driving forces influencing these droplets is limited, although Marangoni instabilities, imbalances in surface tension initiated by symmetry breaking, are thought to play a key role (6). Indeed, along with autocatalytic systems (7–9), chemical gardens (10, 11), and other protocell models (12, 13), these systems together illustrate how the combination of relatively few components and phase boundaries can lead to complex and “life-like” outcomes. Chemotaxis (14, 15) movement in response to chemical stimuli such as a pH or salt concentration gradient has also been observed in simple oil-in-water droplet systems (3, 4, 16–18). These droplet behaviors are thought to be driven by Marangoni instabilities originating from surface tension asymmetry and by the relative solubilities of the oil and aqueous-phase components (6, 19).

The use of automation and image analysis in the exploration of protocell and droplet systems has been shown to be a powerful way to investigate the behaviors observed for a four-component oil-in-water droplet system (2). This is because these platforms are now easy to design and construct using

affordable and open-source hardware and software. For example, bespoke closed-loop systems can be used for the robotic exploration and assisted evolution of physicochemical systems, expanding from the fields of engineering and robotics, and inspired from the realm of biology (20–24). The variation in droplet behaviors as their composition varies can be vast and unpredictable, despite having only a small number of inputs. For example (2), when using only four oil inputs droplets could move rapidly, remain stationary, divide into many smaller droplets, deform, or display a whole range of behaviors. The issue is that the systems seem so complex that deriving mechanistic and predictive information seems far from reach, especially when utilizing smart-automation or standard chemical analytical techniques alone.

Herein, we first apply classic analytical chemistry techniques and machine learning to try to expand understanding of our oil-in-water droplet system and to develop analytical methods universally applicable to such systems. The droplets are composed of four oils [octanoic acid, diethyl phthalate (DEP), 1-octanol, and 1-pentanol] and are placed in a high-pH surfactant-containing aqueous phase. The utilization of machine learning for the prediction of the surface tension and viscosity of the oil mixtures enables the correlation of these to droplet behaviors, and unlocks the dataset collected during optimization to enable mechanistic insight. pH indicators are shown to be a method suitable for visualizing the flow of material within and outside the oil droplets while <sup>1</sup>H NMR spectroscopy is used to quantify the level of oil dissolution in the aqueous phase. Furthermore, we present a chemorobotic platform developed to allow us to study how the chemical environment of the droplets (i.e., the aqueous phase)

## Significance

Exploring and understanding the emergence of complex behaviors is difficult even in “simple” chemical systems since the dynamics can rest on a knife edge between stability and instability. Herein, we study the complex dynamics of a simple protocell system, comprising four-component oil droplets in an aqueous environment using an automated platform equipped with artificial intelligence. The system autonomously selects and performs oil-in-water droplet experiments, and then records and classifies the behavior of the droplets using image recognition. The data acquired are then used to build predictive models of the system. Physical properties such as viscosity, surface tension, and density are related to behaviors, as well as to droplet behavioral niches, such as collective swarming.

Author contributions: J.G. and L.C. designed research; L.J.P., J.W.T., J.G., and K.D. performed research; L.J.P., J.W.T., and K.D. contributed new reagents/analytic tools; L.J.P., J.W.T., and J.G. analyzed data; and L.J.P., J.G., and L.C. wrote the paper.

The authors declare no conflict of interest.

This article is a PNAS Direct Submission.

Published under the PNAS license.

<sup>1</sup>To whom correspondence should be addressed. Email: lee.cronin@glasgow.ac.uk.

This article contains supporting information online at [www.pnas.org/lookup/suppl/doi:10.1073/pnas.1711089115/-DCSupplemental](http://www.pnas.org/lookup/suppl/doi:10.1073/pnas.1711089115/-DCSupplemental).



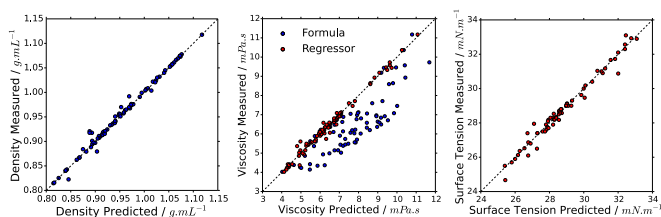


**Fig. 3.** Plots of the predicted density (*Left*), dynamic viscosity (*Center*), and surface tension (*Right*) against their measured values. Blue points are predicted using weighted mean (density) and Arrhenius-based method (viscosity) while red values are predicted using an SVM regressor.

In some cases droplets expel white or pink material and influence the behavior of nearby droplets, suggesting that matter expelled from the droplets affected the Marangoni forces resulting in chemotaxis. This visualization of the “tethering” of droplets is both interesting and surprising. The indicator observations were fairly consistent for the same formulation, but different formulations with a high fitness for a particular behavior did not exhibit identical indicator phenomena.

Hypothesizing that oil dissolution could play a role in droplet behavior, we developed an experimental procedure to quantify the amount of each oil dissolved in the bulk aqueous phase. Interestingly, ethanol was present in the aqueous phase, due to the hydrolysis of DEP, showing that, even in this simple system, both physical and chemical processes take place. Initially, we focused on droplets containing either a single oil or a 1:1 (vol/vol) mixture of two oils.

As can be seen from Fig. 5, there are significant variations in the levels of oil dissolution depending on the oil formulation present. When placed alone, octanoic acid and pentanol dissolve to significant levels (red and purple circles), while DEP is not seen to dissolve at all (blue circle), as expected given the oils’ aqueous solubilities. The trends for the binary mixtures are not, however, as predictable. Octanoic acid and pentanol promote the dissolution of the other oils, while simultaneously their own dissolution is lower. Octanoic acid is seen to dissolve at low levels when mixed with DEP, octanol, or even pentanol. These observations could either be due to molecular-scale interactions or due to droplet behavior. On observing how each of the binary oil droplets behaves, however, there does not appear to be a direct link between oil dissolution and droplet behavior in these cases. For those cases with large error bars, it is thought this is due to spatiotemporal variations in the oil concentration within each experiment.

For full formulations the levels of oil dissolution are similar, but for a few outliers. These formulations represent a vast range of droplet behaviors, thus implying that the level of oil dissolution does not play a key role in defining droplet behavior. There are some exceptions, however. For example, three formulations show significantly higher levels of octanoic acid dissolution than the rest of the formulations. On viewing the phenolphthalein indicator movies of these formulations, these are also the only formulations that show a tethering interaction between droplets, thus implying there is a link between octanoic acid dissolution and this interaction, potentially with octanoic acid aqueous-phase supramolecular assemblies playing a key role. The level of pentanol dissolution is also seen to vary significantly, although in almost all cases this is just a reflection of the changing level of pentanol in the formulation, as pentanol has a relatively high water solubility. It is very surprising to learn that oil dissolution does not play a key role in the quantified droplet behaviors, but can be linked to other observed effects, especially given the fact that oil dissolution was previously thought to be one of the key drivers for symmetry breaking and droplet behavior in this and other systems (2).

**Automated Experiments.** To investigate how the chemical environment of the droplets (i.e., the aqueous phase) influences their behavior, we wished to enable the simultaneous variation and optimization of both the aqueous and oil phases. A robotic

platform was designed to automatically undertake droplet experiments with variable aqueous and oil phases, with droplet analysis via video recording (*SI Appendix, Fig. S11 and Movie S4*). Six aqueous-phase modifiers were chosen for use on the automated platform: the cationic surfactants TTAB and CTAB; the nonionic surfactants Brij O10 and Triton X-100; the zwitterionic surfactant DDMAB, and poly(ethylene glycol) ( $M_n = 400$ ). These were chosen due to their varied chemical structures, properties, effects on droplets, and compatibility. To identify the droplet behaviors possible in this system, 393 random recipes were tested. Movement and division, as previously observed with the single aqueous-phase system, were again the most prevalent droplet behaviors. Remarkably, several other behaviors were identified: swarming, fusion, pulsing, and sorting (*Movie S5*).

“Swarming” was observed when the droplets divided into a large number of small droplets, maintaining a close proximity to each other while appearing to move in concert, as illustrated in Fig. 6. Interestingly, if a larger droplet approached the swarm of smaller droplets, the direction and shape of the whole swarm changed in response to repulsive interactions. From our analysis work we have some understanding of the driving forces behind this swarming behavior. Initially, a large number of droplets must be present—hence the formulation must be unstable, leading to rapid division. Following this, small droplets either move collectively, apparently driven by bulk surface tension variations “carrying” the droplets together, or the smaller droplets are “herded” by larger droplets, whose more definite movements through the swarm cause the swarm to shift around the larger droplet. Often, there is a period of rapid division at the beginning of the experiment followed by a period of swarming and then the repeated fusion of the small droplets.

Droplet “fusion” had previously been observed in the TTAB-only system, but it was very rare owing to the stabilizing boundary formed by the cationic surfactant. It would, however, be a desirable behavior for oil droplets to exhibit, especially if it can be controlled, due to the possibility of controlling a chemical reaction between two components dissolved in two separate

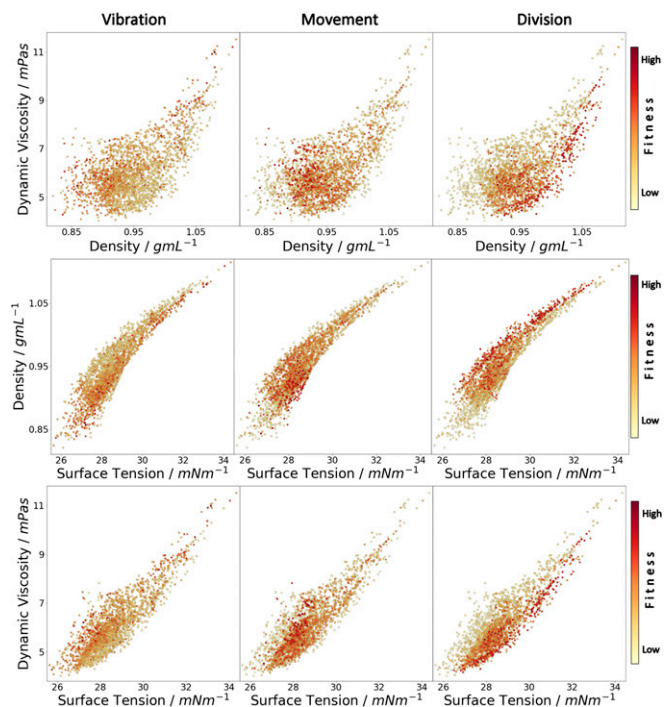


**Fig. 4.** Impact of dynamic viscosity, density, and surface tension on droplet behavior: movement (*Left*), vibration (*Center*), and division (*Right*). Each dot is an experiment; the color is proportional to the intensity of the behavior.

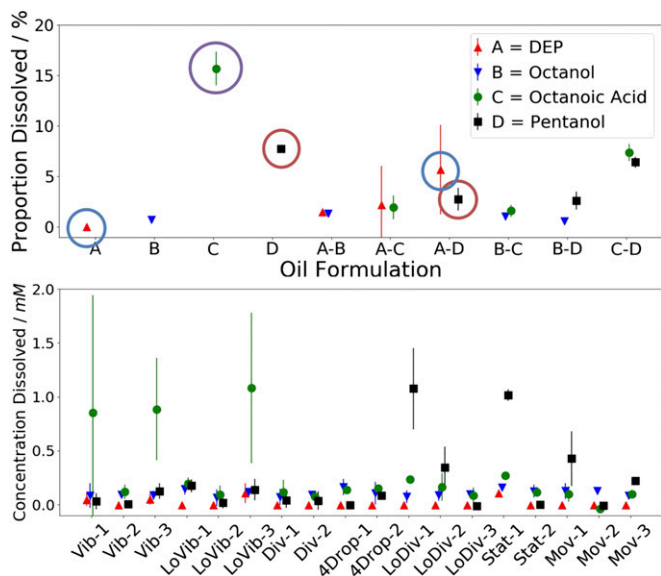


**Fig. 5.** Plots showing the concentration of oil dissolved in the aqueous phase for various formulations 1 min after  $4 \times 4 \mu\text{L}$  droplets are placed in 3.5 mL aqueous phase. (Top) The proportion of the oil present dissolved for droplets composed of a single oil or 1:1 (vol/vol) mixture of two oils, i.e., point A-B, corresponds to the oil-dissolution levels when a 1:1 (vol/vol) mixture of DEP and octanol is used as the droplet formulation. (Bottom) The concentration oil dissolved for full four-oil formulations, categorized by the high- or low fitnesses they show for certain behaviors. Key: Vib, LoVib: high or low vibration fitness. Div, LoDiv: high or low division fitness. 4Drops: division fitness of 4; i.e., four droplets present after 1 min. Mov, Stat: high or low movement fitness. Error bars show SD.

droplets. Electrostatic repulsion plays a role in the prevention of fusion, in addition to surfactant gradients induced by the decrease of distance between droplets resulting in Marangoni forces against the direction of movement (30). These forces can be reduced by ion pairing between oppositely charged ions (e.g., quaternary ammonium surfactant and octanoate). Clusters of many smaller droplets provide greater surface area for the deprotonation of octanoic acid, which combined with cationic surfactants in the aqueous phase forms a catanionic system. Indeed, fusion is far more commonly observed for smaller droplets and division for larger droplets, implying there may be an intermediate optimal radius in many cases. As surfactant concentrations vary, fluctuations in interfacial tension mean that division could be favored in one location in the dish and fusion in another (31). Some droplet formulations give droplets which may fuse if they happen by chance to collide with each other, i.e., they have no significant repulsive or attractive forces, while others exhibit attraction to each other and experience a change of trajectory before fusion. “Pulsing” droplets exhibit constant, rapid changes in diameter as the droplets shrink and grow periodically. This is in contrast to vibration, which involves rapid changes in a droplet’s direction of movement. When droplets were attracted to the walls of the Petri dish they sometimes also exhibited movement around the edge of the dish, division or fusion. This also often resulted in droplet “sorting,” in which the droplets spread themselves evenly around the circumference of the dish due to repulsive interactions between the droplets.

Having identified the behaviors possible in this system, a genetic algorithm optimization was then carried out for movement using all 10 components. CTAB and Brij-O10 were quickly optimized out almost entirely (SI Appendix, Fig. S10); thus, only the remaining four aqueous phases were subsequently used. It is very interesting to note that TTAB and CTAB, which differ only by two  $\text{CH}_2$  groups to the surfactant tail, have such different effects on droplet behavior. The results of a genetic algorithm optimization for movement (average

speed of the droplets) with these eight parameters are shown in Fig. 7.4. With these eight inputs there are  $9.2 \times 10^{15}$  possible recipes, a space unfeasible to search exhaustively. The genetic algorithm was run for 30 generations, with 10 new recipes each generation, taking  $\sim 80$  h for a complete optimization. The optimization was repeated in triplicate from random starting recipes, and compared with the maximum fitness values observed in the oil-only experiments. The final median fitness value of each individual genetic algorithm run surpassed  $5.37 \text{ mm s}^{-1}$ , while the maximum fitness value achieved was  $9.59 \text{ mm s}^{-1}$ . This compares to the oil-only optimizations which achieved a maximum droplet speed of  $7.17 \text{ mm s}^{-1}$  and a median of up to  $4.78 \text{ mm s}^{-1}$ . The large increase in median fitness from less than 1.0 up to  $5.37$ – $6.93 \text{ mm s}^{-1}$  showed that the environment in which the droplets are placed has a considerable influence on their movement, and that the higher number of parameters used in the optimization enabled even higher fitnesses to be observed. SI Appendix, Fig. S13 shows the evolution of the composition of both the aqueous and oil phases during the evolutionary experiments. Overall, the compositional trajectories and final values differ significantly between runs while the upward trend in fitness is conserved, illustrating the complexity of the system and why it is beneficial to optimize the aqueous and oil phases together. Interestingly, as SI Appendix, Fig. S14 shows, the physical properties of the oil phase are fairly consistent throughout the runs, despite this compositional variation.

To investigate whether such high fitnesses could be observed by first optimizing the oil phase and then the aqueous phase, instead of optimizing them simultaneously, evolution experiments were carried out with a predefined high-fitness oil formulation optimized in the TTAB-only aqueous phase (SI Appendix, Fig. S15). The recipe chosen had a high, reproducible movement fitness value of  $5.96 \text{ mm s}^{-1}$ . The oil droplet fitness again increased throughout the optimization, but only by  $1$ – $2 \text{ mm s}^{-1}$ , in contrast to  $\sim 6.0 \text{ mm s}^{-1}$  in the case of the eight-parameter evolution experiment. Only one of the three runs surpassed the fitness previously observed with 100% TTAB aqueous phase, suggesting that 100% TTAB was close to the optimal aqueous phase for this oil formulation, even though much higher fitnesses are attainable with different oil–aqueous formulations. Movie S6 compares the fastest-moving droplets from each of these evolution experiments.

The evolutionary trajectories were compared between the oil-only, aqueous-only, and combined optimizations (Fig. 7.4). The oil-only

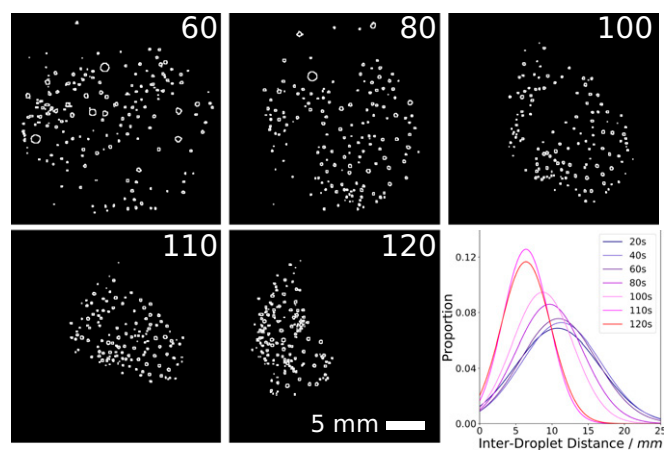


**Fig. 6.** Movie snapshots of a swarming formulation, converted into black and white outlines using ImageJ. Numbers in the corners correspond to the experiment time in seconds since the experiment started. Initially there are relatively few droplets, fairly evenly spaced (0–60 s). These then divide and swarm, to give more droplets closer together. At around 100–105 s, the rapid dissolution of a droplet stuck to the edge of the dish (not shown) leads to a much tighter-knit swarm, with an average interdroplet distance of only around 6.4 mm. The variation in interdroplet distance is also seen to decrease. Images processed using ImageJ (29).



**Random Matrix Screen.** A proximity-limited random search was carried out in 10 dimensions (6 aqueous, 4 oils); using a threshold factor to ensure formulations generated were sufficiently different, 393 random formulations were tested.

**Genetic Algorithm Explorations.** A genetic algorithm was used with a genome length equal to the number of components for the mixture. Twenty-four random combinations were tested to form generation 1, then roulette wheel selection was used to select individuals carried over to undergo cross-over and random mutation—forming the next generation of 10 individuals. The experiment was continued for 30 generations. An individual's fitness was quantified using the previously published methodology (2).

1. Lach S, Yoon SM, Grzybowski BA (2016) Tactic, reactive, and functional droplets outside of equilibrium. *Chem Soc Rev* 45:4766–4796.
2. Gutierrez JMP, Hinkley T, Taylor JW, Yanev K, Cronin L (2014) Evolution of oil droplets in a chemorobotic platform. *Nat Commun* 5:5571.
3. Hanczyc MM, Toyota T, Ikegami T, Packard N, Sugawara T (2007) Fatty acid chemistry at the oil-water interface: Self-propelled oil droplets. *J Am Chem Soc* 129:9386–9391.
4. Lagzi I, Soh S, Wesson PJ, Browne KP, Grzybowski BA (2010) Maze solving by chemotactic droplets. *J Am Chem Soc* 132:1198–1199.
5. Dzieciol AJ, Mann S (2012) Designs for life: protocell models in the laboratory. *Chem Soc Rev* 41:79–85.
6. Schmitt M, Stark H (2016) Marangoni flow at droplet interfaces: Three-dimensional solution and applications. *Phys Fluids* 28:12106.
7. Bissette AJ, Odell B, Fletcher SP (2014) Physical autocatalysis driven by a bond-forming thiol-ene reaction. *Nat Commun* 5:4607.
8. Ortega-Arroyo J, Bissette AJ, Kukura P, Fletcher SP (2016) Visualization of the spontaneous emergence of a complex, dynamic, and autocatalytic system. *Proc Natl Acad Sci USA* 113:11122–11126.
9. Bottero I, Huck J, Kosikova T, Philp D (2016) A synthetic replicator drives a propagating reaction-diffusion front. *J Am Chem Soc* 138:6723–6726.
10. Haudin F, Cartwright JHE, Brau F, De Wit A (2014) Spiral precipitation patterns in confined chemical gardens. *Proc Natl Acad Sci USA* 111:17363–17367.
11. Barge LM, et al. (2015) From chemical gardens to chemobionics. *Chem Rev* 115:8652–8703.
12. Qiao Y, Li M, Booth R, Mann S (2017) Predatory behaviour in synthetic protocell communities. *Nat Chem* 9:110–119.
13. Engelhart AE, Adamala KP, Szostak JW (2016) A simple physical mechanism enables homeostasis in primitive cells. *Nat Chem* 8:448–453.
14. Adler J, Tso W-W (1974) "Decision"-making in bacteria: Chemotactic response of *Escherichia coli* to conflicting stimuli. *Science* 184:1292–1294.
15. Van Haastert PJM, Devreotes PN (2004) Chemotaxis: Signalling the way forward. *Nat Rev Mol Cell Biol* 5:626–634.
16. Toyota T, Maru N, Hanczyc MM, Ikegami T, Sugawara T (2009) Self-propelled oil droplets consuming "fuel" surfactant. *J Am Chem Soc* 131:5012–5013.
17. Miura S, et al. (2014) pH-induced motion control of self-propelled oil droplets using a hydrolyzable gemini cationic surfactant. *Langmuir* 30:7977–7985.
18. Cejková J, Novák M, Stepánek F, Hanczyc MM (2014) Dynamics of chemotactic droplets in salt concentration gradients. *Langmuir* 30:11937–11944.
19. Scriven LE, Sterling CV (1960) The Marangoni effects. *Nature* 187:186–188.
20. Eiben AE, Kernbach S, Haasdijk E (2012) Embodied artificial evolution: Artificial evolutionary systems in the 21st century. *Evol Intell* 5:261–272.
21. Harding SL, Miller JF, Rietman EA (2008) Evolution in materio: Exploiting the physics of materials for computation. *Int J Unconv Comput* 4:155–194.
22. Hornby GS, Lohn JD, Linden DS (2011) Computer-automated evolution of an X-band antenna for NASA's Space Technology 5 mission. *Evol Comput* 19:1–23.
23. Eiben AE, Smith J (2015) From evolutionary computation to the evolution of things. *Nature* 521:476–482.
24. Gould SJ (1982) Darwinism and the expansion of evolutionary theory. *Science* 216:380–387.
25. Jordan MI, Mitchell TM (2015) Machine learning: Trends, perspectives, and prospects. *Science* 349:255–260.
26. Raccuglia P, et al. (2016) Machine-learning-assisted materials discovery using failed experiments. *Nature* 533:73–76.
27. Carleo G, Troyer M (2017) Solving the quantum many-body problem with artificial neural networks. *Science* 355:602–606.
28. Smith JS, Isayev O, Roitberg AE (2017) ANI-1: An extensible neural network potential with DFT accuracy at force field computational cost. *Chem Sci (Camb)* 8:3192–3203.
29. Schneider CA, Rasband WS, Eliceiri KW (2012) NIH Image to ImageJ: 25 years of image analysis. *Nat Methods* 9:671–675.
30. Baret J-C (2012) Surfactants in droplet-based microfluidics. *Lab Chip* 12:422–433.
31. Caschera F, Rasmussen S, Hanczyc MM (2013) An oil droplet division-fusion cycle. *ChemPlusChem* 78:52–54.
32. Lehman J, Stanley KO (2008) Exploiting open-endedness to solve problems through the search for novelty. *Proceedings of the Eleventh International Conference on Artificial Life (ALIFE XI)* (MIT Press, Cambridge, MA), pp 329–336.
33. Oudeyer PY, Kaplan F, Hafner VV (2007) Intrinsic motivation systems for autonomous mental development. *IEEE Trans Evol Comput* 11:265–286.

**ACKNOWLEDGMENTS.** We thank Dr. Salah Sharabi for assistance with hardware and electronics, Dr. Sergey Zaleskiy for assistance with <sup>1</sup>H NMR spectroscopy experiments, Kliment Yanev for providing the base platform, and Dr. Juan Manuel Parrilla Gutierrez. We gratefully acknowledge financial support from the Engineering and Physical Sciences Research Council (EPSRC) for funding (Grants EP/H024107/1, EP/I033459/1, EP/J00135X/1, EP/J015156/1, EP/K021966/1, EP/K023004/1, EP/K038885/1, EP/L015668/1, and EP/L023652/1), the Biotechnology and Biological Sciences Research Council (BBSRC) (Grant BB/M011267/1), and the European Commission (EC) (Projects 610730 EVOPROG and 611640 EVOBLISS). L.C. thanks the Royal Society/Wolfson Foundation for a Merit Award and the European Research Council (ERC) for an Advanced Grant (ERC-ADG, 670467 SMART-POM).